

# Vanishing Hysteresis in Carbon Nanotube Transistors Embedded in Boron Nitride/Polytetrafluoroethylene Heterolayers

Sandeep Kumar,\* Daghan Dagli, Simone Dehm, Chittaranjan Das, Li Wei, Yuan Chen, Frank Hennrich, and Ralph Krupke\*

Carbon nanotube field-effect transistors fabricated on silicon wafers with thermal oxide often suffer from large gate-voltage hysteresis, induced by charge trapping sites in oxides, surface hydroxyl groups, and the presence of water molecules. Surface functionalization and passivation, as well as vacuum annealing and reduced operating temperature, have shown to diminish or even eliminate hysteresis. Herein, the fabrication of nearly hysteresis-free transistors on Si/SiO<sub>2</sub> by embedding carbon nanotubes and the connecting electrodes in a hexagonal boron nitride (h-BN) bottom layer and a polytetrafluoroethylene (PTFE) top layer is demonstrated. The conditions at which catalyst-free synthesis of h-BN on SiO<sub>2</sub>/Si with borazine is obtained, and the subsequent liquid-phase deposition of PTFE, are discussed. Device transfer curves are measured before and after PTFE deposition. It is found that the hysteresis is reduced after PTFE deposition, but vanishes only after a waiting period of several days. Simultaneously, the on-state current increases with time. The results give evidence for the absence of trap states in h-BN/PTFE heterolayers and a high breakthrough field strength in those wafer-scalable materials.


traps in dielectric layer,<sup>[6]</sup> or charging of surface hydroxyl (–OH) groups.<sup>[7]</sup> The key toward hysteresis-free SWCNT transistors is to form a nanotube environment that is free of trap states and water molecules. Placing SWCNTs onto oxides functionalized with silanes,<sup>[8]</sup> or hydrophobic dielectric layers such as Parylene<sup>[9]</sup> or polytetrafluoroethylene (PTFE),<sup>[10]</sup> greatly reduces p-doping and hysteresis induced by surface –OH groups, in analogy to observations with organic semiconductors.<sup>[11]</sup> Furthermore, coating SWCNTs with poly(methyl methacrylate) polymers or methyl siloxane polymers can provide the water repellent packaging required for suppressing water-induced hysteresis.<sup>[4,7,12–15]</sup> Also, growing on SWCNTs, a thin oxide layer below a top-gate metal can greatly reduce hysteresis,<sup>[16]</sup> although often a transparent top layer with a bottom-gate is preferred. An example of

Transistors based on single-walled carbon nanotubes (SWCNTs) have been extensively studied since their realization by Dekker and co-workers<sup>[1]</sup> and Avouris and co-workers.<sup>[2]</sup> Also, although not shown in all works, hysteresis is observed as an omnipresent feature, which can be useful for memory applications,<sup>[3]</sup> however in most cases is unwanted. Several works have identified that hysteresis is induced by water molecules,<sup>[4,5]</sup> filling and depleting

hysteresis-free SWCNT bottom-gate transistors fabricated on SiO<sub>2</sub>/Si wafers has been demonstrated by Javey and co-workers via a combination of surface functionalization and PTFE coating.<sup>[17]</sup> Removal of hysteresis has also been shown by Weitz et al. by growing a self-assembled monolayer on an Al gate electrode.<sup>[18]</sup> Yet in practice, while fabricating back-gated SWCNT transistors on SiO<sub>2</sub>/Si wafers, these measures do not

S. Kumar, D. Dagli, S. Dehm, Prof. R. Krupke  
Institute of Nanotechnology  
Karlsruhe Institute of Technology  
76021 Karlsruhe, Germany  
E-mail: sandeep.kumar@partner.kit.edu; krupke@kit.edu

S. Kumar, D. Dagli, Prof. R. Krupke  
Institute of Materials Science  
Technische Universität Darmstadt  
64287 Darmstadt, Germany

 The ORCID identification number(s) for the author(s) of this article can be found under <https://doi.org/10.1002/pssr.202000193>.

© 2020 The Authors. Published by WILEY-VCH Verlag GmbH & Co. KGaA, Weinheim. This is an open access article under the terms of the Creative Commons Attribution License, which permits use, distribution and reproduction in any medium, provided the original work is properly cited.

DOI: 10.1002/pssr.202000193

Dr. C. Das  
Institute of Applied Materials  
Karlsruhe Institute of Technology  
76021 Karlsruhe, Germany

Dr. L. Wei, Prof. Y. Chen  
School of Chemical and Biomolecular Engineering  
The University of Sydney  
Sydney, NSW 2006, Australia

Dr. F. Hennrich, Prof. R. Krupke  
Institute of Quantum Materials and Technology  
Karlsruhe Institute of Technology  
76021 Karlsruhe, Germany

always eliminate hysteresis completely, potentially due to the defects in the self-assembled layers, oxides or coatings, or due to water molecules trapped at the metal contacts<sup>[19–21]</sup> or within the nanotubes.<sup>[22]</sup> Suspending carbon nanotubes and exposing to high vacuum,<sup>[5]</sup> or cooling to 4 K can eliminate hysteresis completely,<sup>[23]</sup> albeit these measures are limiting the applicability. In contrast, the graphene community has realized that packaging graphene into flakes of hexagonal boron nitride (h-BN) eliminates doping and hysteresis, and boosts mobility, provided that the h-BN layer is tens of nanometers thick.<sup>[24]</sup> Bockrath and co-workers have similarly encapsulated SWCNT devices in h-BN flakes and reported superior current carrying capability;<sup>[25]</sup> however, the integrated nanotubes were metallic, and transistor behavior was not observed, also not for SWCNTs grown on h-BN flakes.<sup>[26]</sup> Herein, we have been targeting a wafer-scalable fabrication of hysteresis-free SWCNTs transistors via encapsulation into a h-BN bottom layer and a PTFE top layer. The h-BN layer was grown on SiO<sub>2</sub>/Si wafers by a catalyst-free chemical vapor deposition with borazine as precursor. The devices based on solution phase-purified (9,8) SWCNTs were built on top of the h-BN/SiO<sub>2</sub>/Si substrates using dielectrophoresis (DEP), and subsequently coated by liquid-phase deposition of PTFE. We report on the h-BN synthesis, the impact of the bottom and top layers on the device characteristics, and evolution with time.

The synthesis of large-area h-BN has been demonstrated in previous works by the decomposition of ammonia borane or borazine on metal foils,<sup>[27–31]</sup> on dielectric surfaces,<sup>[32,33]</sup>

and by chemical conversion of graphene to h-BN.<sup>[34]</sup> Herein, we decided to avoid transfer processes which are often accompanied with the formation of wrinkles, defects, and impurities, and grew h-BN directly on the SiO<sub>2</sub>/Si surface. The process flow in cross-sectional view and the methods used are schematically shown in **Figure 1a,b**. We used borazine as a stoichiometric precursor because of its high vapor pressure and chemical reactivity.<sup>[28,29,35]</sup> A stainless-steel bubbler (100 mL) filled with borazine (5 g) (Katchem, Czech Republic) was connected to an Ar gas bottle (Linde, purity 5 N), and to a high-vacuum oven (Gero, heating zone diameter: 7 cm, length: 65 cm) via a mass flow controller (MKS 1179B). The bubbler was cooled to 5 °C to inhibit decomposition of borazine. Boron-doped silicon wafers (resistance <0.005 Ω cm, Active Business Company) with 300 nm thermal oxide were cut into 10 × 10 mm<sup>2</sup> pieces, loaded into the center of a quartz tube (Aachener Glas, 2 in. diameter, 50 cm long), evacuated to 10<sup>−7</sup> mbar and ramped up to 1000 °C at a rate of 10 °C min<sup>−1</sup>. Argon (2 sccm) was flown through the borazine-filled bubbler into the heated quartz tube for 10–60 min, depending on the targeted h-BN thickness. We have estimated the flow of borazine through the oven to 1 mg min<sup>−1</sup> at 2 sccm Ar flow, assuming that Ar uptakes borazine to the equilibrium partial pressure of 144 mbar at 5 °C when streaming through the bubbler at 1 bar pressure. During growth, a pressure of 5 mbar was maintained by reducing the pump speed. After terminating the gas flow, the sample was kept in vacuum at 1000 °C for 1 h to improve crystallinity and to promote further

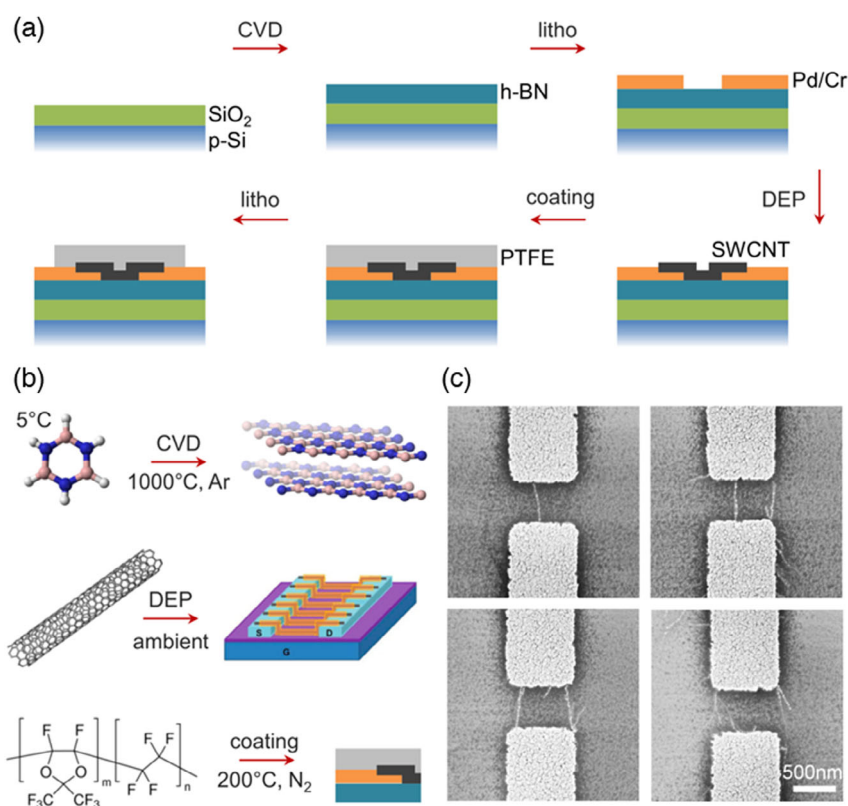


**Figure 1.** a) Process flow comprising CVD synthesis of h-BN, deposition of SWCNTs by DEP, spin coating of Teflon AF2400 (PTFE), and lithographic patterning of metal contacts and Teflon layer. b) Schematic on the deposition processes and conditions. c) Scanning electron micrographs of devices after deposition of (9,8) SWCNTs and before Teflon coating. The SiO<sub>2</sub>/Si substrate was overgrown with 80 nm h-BN.

dehydrogenation. Finally, the furnace was cooled to room temperature (RT) at a rate of  $<7\text{ }^{\circ}\text{C min}^{-1}$ . To avoid premature polymerization of borazine to polyborazylene,<sup>[36]</sup> we have ensured to keep the gas temperature in the gas pipes to below  $70\text{ }^{\circ}\text{C}$ . In the heating zone, two additional dehydrogenation steps occur: at  $125\text{--}300\text{ }^{\circ}\text{C}$  with cross-linking of B—H and N—H and at  $700\text{--}1000\text{ }^{\circ}\text{C}$  ultimately forming BN.<sup>[37]</sup> The h-BN films were characterized by Raman spectroscopy with 532 nm laser excitation at 60 mW power (Renishaw inVia Microscope), and by reflectometry under normal incidence (Filmetrics F20). X-ray photoelectron spectroscopy (XPS) measurements were done using a Thermo Fisher's K-alpha machine. The samples were excited with monochromatized Al K-alpha source (1486.6 eV) with an X-ray spot size of  $400\text{ }\mu\text{m}$ . The ejected photoelectrons were collected using a hemispherical  $180^{\circ}$  double-focus analyzer with 128-channel detector. The measurements were done without the use of the charge compensation mechanism.

The 45 nm-thick Pd/Cr source drain electrodes with 600 nm gap size were fabricated on the h-BN-coated substrates by standard electron-beam lithography and metallization. The (9,8) semiconducting SWCNTs were produced by selective catalyst chemical vapor deposition,<sup>[38,39]</sup> dispersed in toluene by wrapping in poly(9,9-di-*n*-dodecylfluorenyl-2,7-diyl) (PFD), and

purified and length sorted by gel filtration.<sup>[40]</sup> The SWCNTs were deposited simultaneously onto 6–7 devices per chip by electric field-assisted deposition (DEP). For details regarding synthesis, purification, optical characterization, and deposition of (9,8) SWCNTs, we refer to Gaulke et al.<sup>[23]</sup> Devices were then annealed at  $400\text{ }^{\circ}\text{C}$  and  $10^{-7}$  mbar vacuum for 4 h. Electrical characterization was conducted first without PTFE top layer under ambient conditions, with an Agilent 4155C semiconductor parameter analyzer and a probe station with TRIAX probes with a current detection limit of 30 fA. Transfer characteristics were measured with back-gate voltage sweeps from  $-5$  to  $+5\text{ V}$  (step size 100 mV, scan rate  $0.5\text{ V s}^{-1}$ ) using source-drain voltages of 0.5 V. For coating PTFE, the devices were loaded into a nitrogen glove box with a spin-coater and hotplate and annealed at  $150\text{ }^{\circ}\text{C}$  for 1 h. A solution of poly[4,5-difluoro-2,2-bis(trifluoromethyl)-1,3-dioxole-co-tetrafluoroethylene] (1 g) (Teflon AF-2400, Sigma-Aldrich) dissolved in Fluorinert FC-40 (100 mL) (Sigma-Aldrich) was prepared by stirring the solution for 2 weeks at  $60\text{ }^{\circ}\text{C}$ . Residual nanometer-sized PTFE particles were removed by ultracentrifugation for 1 h at 40 000 rpm. The devices were loaded to the spin-coater and purified 1% PTFE solution (10  $\mu\text{L}$ ) was drop-casted onto the sample surface. For 30 and 45 nm-thick PTFE layers, the samples were rotated for 60 s at 3000 and 1000 rpm,

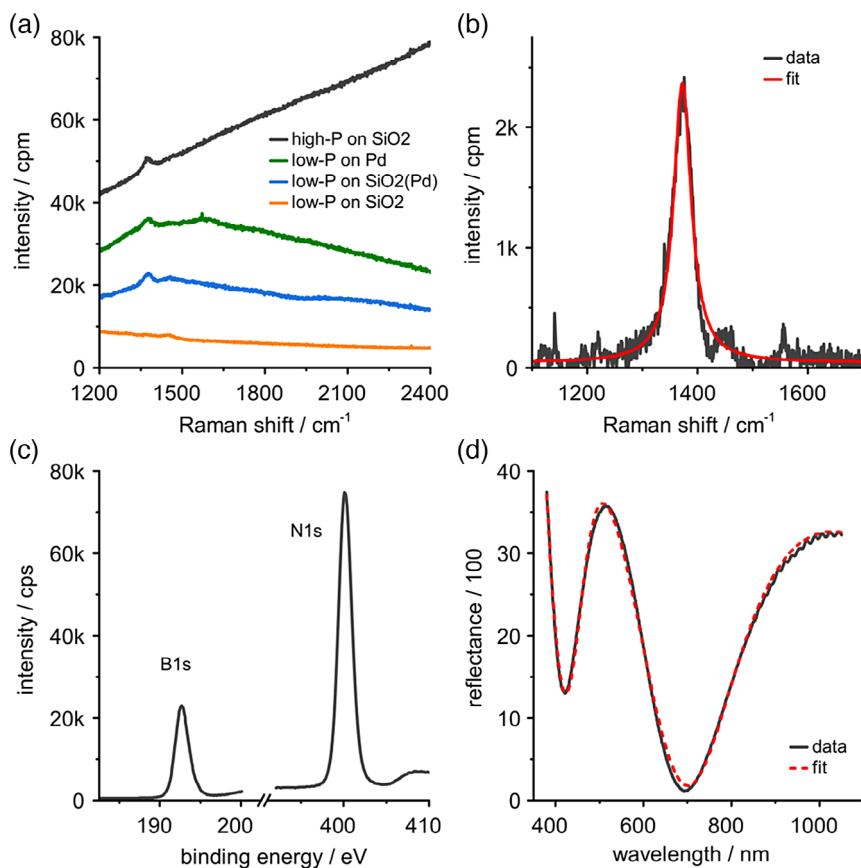


**Figure 2.** a) Raman spectra recorded after CVD. The  $E_{2g}$  Raman peak of h-BN is visible on bare  $\text{SiO}_2/\text{Si}$  substrates when synthesized at high pressure (5–10 mbar, black line). Synthesis at low pressure ( $10^{-6}$  mbar) yields h-BN only in the presence of Pd electrodes: on top of Pd (green line) and nearby Pd (blue line), not on bare substrates (orange). b) Raman data of high pressure grown h-BN on  $\text{SiO}_2/\text{Si}$ , background subtracted and fitted to a Lorentzian (peak  $1372.5\text{ cm}^{-1}$ , linewidth  $38.7\text{ cm}^{-1}$ ). c) XPS of the h-BN film with the peak binding energies for B 1s and N 1s at 192 and 399.5 eV, respectively. d) Reflectance spectra of a complete stack of 30 nm Teflon/40 nm h-BN/300 nm  $\text{SiO}_2/\text{Si}$  determined by fitting with the transfer matrix method.

respectively. A thickness of 80 nm was obtained by spin-casting two times, at 3000 and 1000 rpm for 60 s each. The samples were then heated—still in nitrogen atmosphere—at 100 °C for 5 min, 150° for 5 min, and 200 °C for 10 h. Finally, the samples were cooled down to RT and unloaded from the glovebox. PTFE was removed from the metal contact pads by direct electron beam patterning using an exposure dose of 10 mC cm<sup>-2</sup> at 10 keV beam energy.<sup>[41]</sup> Subsequent electrical characterizations were done under the conditions outlined before. At the end of the fabrication process, the SWCNT devices are encapsulated between the h-BN bottom and PTFE top layer (Figure 1a). SWCNTs within completed devices cannot be imaged due to the PTFE coating; therefore, we show in Figure 1c scanning electron micrographs of four representative SWCNT devices without PTFE coating. The images were recorded after nanotube DEP. Typically, 1–5 SWCNTs are contacted and visible in the gap region. The underlying h-BN layer was characterized by Raman spectroscopy after the chemical vapor deposition (CVD) synthesis and results are shown in Figure 2a for synthesis at 5 and 10<sup>-6</sup> mbar pressure, on bare SiO<sub>2</sub>/Si substrates and on substrates with Pd patches. At high pressure and on the bare substrate, the characteristic  $E_{2g}$  Raman peak for h-BN is observed at 1372.5 cm<sup>-1</sup> (linewidth 38.7 cm<sup>-1</sup>), which is consistent with the measurements on monolayer,<sup>[27,34]</sup> multilayer,<sup>[31–33,42,43]</sup> and bulk h-BN.<sup>[27]</sup> The

increasing background is due to photoluminescence and has been subtracted in Figure 2b. At low pressure, h-BN does not form on a bare substrate; however, in the presence of Pd, h-BN grows on Pd and next to Pd on the substrate. Indeed, the growth of h-BN at ultrahigh vacuum conditions has been observed on different single-crystal metals,<sup>[44–46]</sup> whereas here we see that h-BN growth also occurs in the vicinity of a metal. The results that we obtain at high pressure (5 mbar borazine) are in agreement with h-BN synthesis on metal substrates,<sup>[47]</sup> and on dielectric substrates.<sup>[48]</sup> Also, borazine<sup>[49,50]</sup> and ammonia borane<sup>[47,51]</sup> are the most commonly used precursors for h-BN growth due to stoichiometric ratio of B:N being 1:1. The XPS data of an h-BN layer on SiO<sub>2</sub>/Si are shown in Figure 2c. The peak binding energies for B 1s and N 1s at 192 and 399.5 eV, respectively, are also consistent with the formation of h-BN.<sup>[27,29,32,33,35,43]</sup> The complete stack of PTFE/h-BN/SiO<sub>2</sub>/Si has been characterized by reflectance spectroscopy to analyze the thicknesses of the individual layers via the transfer matrix method, as shown in Figure 2d. Refractive indices of PTFE AF-2400<sup>[52]</sup> and PTFE/h-BN,<sup>[53]</sup> and respective nominal thicknesses of the layers were used as starting values in the fitting procedure. The h-BN layers are homogenous over large areas, as shown in optical image in Figure S2, Supporting Information. However, the layers are not single crystalline but have a grainy

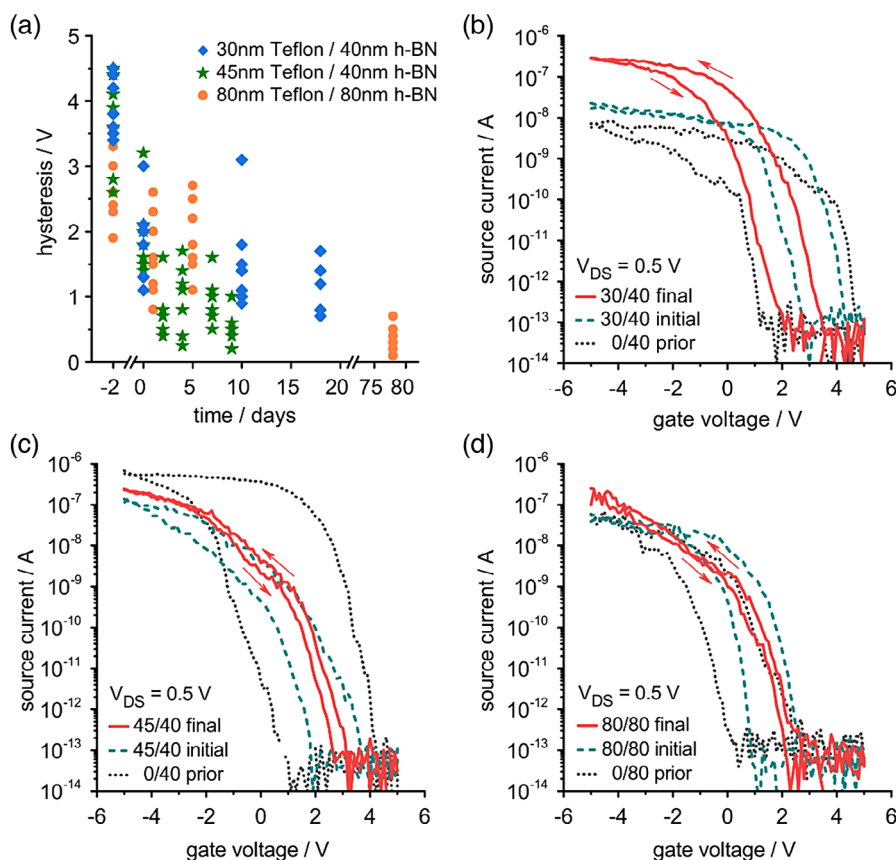


**Figure 3.** a) Temporal evolution of hysteresis in transconductance curves for 21 devices. The SWCNT devices were encapsulated in three combinations of Teflon and h-BN layer thicknesses, as indicated. Also, shown are results taken 2 days before the Teflon deposition at  $t = 0$ . b–d) Corresponding transconductance curves of representative devices, taken before Teflon deposition (prior), directly after Teflon deposition (initial) and after a week of storage under ambient conditions (final). Current detection limit is 30 fA.

structure, which gives rise to a broader linewidth of the Raman  $E_{2g}$  peak ( $38.7\text{ cm}^{-1}$ ) compared with monocrystalline h-BN ( $15.5\text{ cm}^{-1}$  for bulk),<sup>[27]</sup> and is visible in the scanning electron micrographs in Figure S3, Supporting Information.

We discuss now the gate-voltage hysteresis observed in the transconductance curves of h-BN/SiO<sub>2</sub>/Si supported devices before and after Teflon AF coating. The (9,8) devices were embedded in three combinations of layer thicknesses: 30 nm Teflon/40 nm h-BN, 45 nm Teflon/40 nm h-BN, and 80 nm Teflon/80 nm h-BN. **Figure 3a** shows the temporal evolution of the hysteresis of in total 21 devices. The largest hysteresis values among all layer combinations are observed prior to Teflon deposition at  $t = -2$  days ranging between 2 and 4.5 V. This is significantly smaller than the 4.5–6 V range for SWCNT devices fabricated on bare Si/SiO<sub>2</sub> (Figure S1, Supporting Information) and shows that h-BN without Teflon coating yields devices with a reduced hysteresis. An additional reduction of hysteresis to 1–3 V is then observed after Teflon coating at  $t = 0$ , as was expected due to the water repelling nature of Teflon. However, an unexpected further significant reduction is observed over a timescale of days to weeks, in particular for 45 and 80 nm-thick Teflon layers. Depending on the waiting time and the layer combination, the hysteresis becomes eventually smaller than 1 V. A direct comparison of the transconductance curves for representative

devices of the three layer combination is shown in Figure 3b–d. The results resemble similarity to Ha et al.'s work,<sup>[17]</sup> where a vanishing hysteresis has been obtained after Teflon AF coating of SWCNTs on an amino acid-functionalized substrate. The Teflon layers required a thickness larger than 10 nm to be effective; however, the reduction in hysteresis was instantaneous and did not show a time dependence, likewise for a complete encapsulation in Teflon as shown by Lefebvre et al.<sup>[10]</sup> Herein, a minimum Teflon thickness of 45 nm is required to coat not only the SWCNTs segment lying flat on the h-BN surface but also the nanotube segment on the top of the metal electrodes. Concerning the origin of the temporal evolution of the hysteresis, it is the long timescale that points to a diffusion process—likely of water molecules. Interestingly, the transconductance traces show that the threshold voltage is stable during the hysteresis reduction; however, the on-state hole current systematically increases with time after Teflon coating. This shows that the Schottky barrier reduction for holes is correlated with the reduction of hysteresis, possibly via surface dipoles trapped in the contact area between Pd electrodes and SWCNTs. Indeed, an obvious difference to the previous works is that in this work SWCNTs were deposited on top of the Pd electrodes and hence the contact interface was inevitably exposed to humidity. Because water molecules are known to adsorb on Pd surfaces<sup>[21]</sup> and desorption

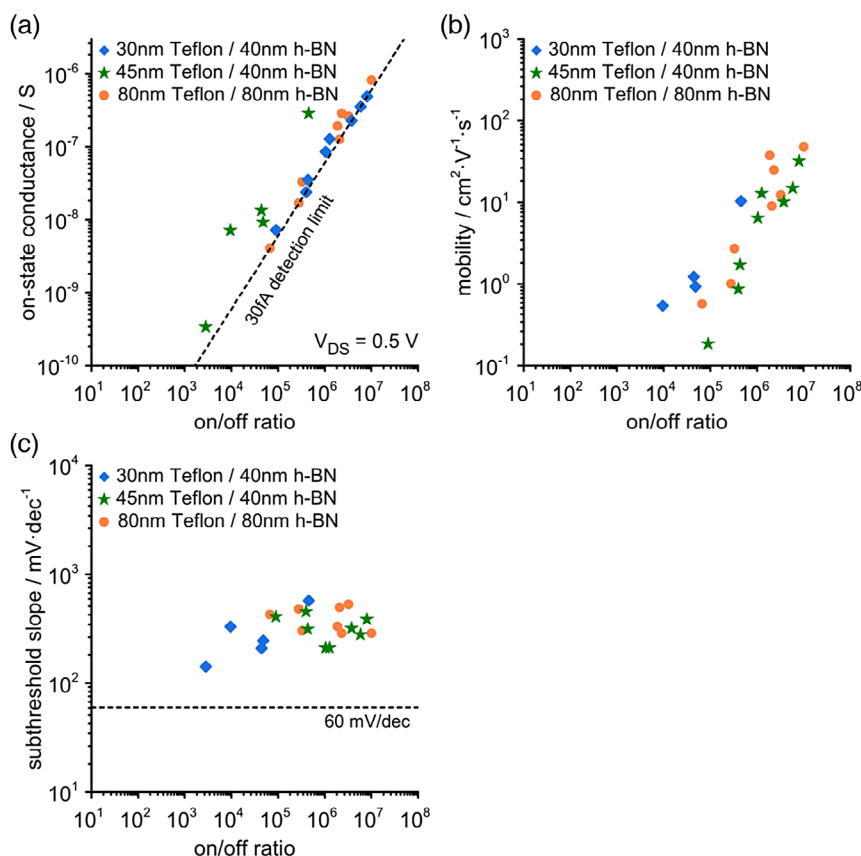


**Figure 4.** a) On-state conductance, b) mobility, and c) subthreshold slope for 21 devices. The SWCNT devices were encapsulated in three combinations of h-BN and Teflon layer thicknesses, as indicated. The data have been acquired from the conductance curves measured after a week of storage under ambient conditions. In part (a), the dashed line represents the 30 fA detection limit of the setup, and in part (c) the theoretical subthreshold slope limit at 300 K.



of water from Pd surfaces is slow below 450 °C,<sup>[54]</sup> we believe that slow repelling of water molecules from the contact area is causing the time dependence. The direction of the hysteresis loop in Figure 3b–d is counterclockwise and further evidences that the source of hysteresis at low gate sweeping ranges is due to water molecules and associated charges, which redistribute in response to the gate voltage.<sup>[55]</sup> At larger gate voltage sweeps, hysteresis may also depend on charge traps in the dielectric; however, in light of the observed reduction of hysteresis with time, we conclude that hysteresis in our devices must be caused by water-related charge traps that are mobile at RT and traps in h-BN are absent. The low hysteresis of 0.1 V observed for devices embedded in 40 nm h-BN/45 nm Teflon and 80 nm h-BN/80 nm Teflon on SiO<sub>2</sub> substrates is comparable with devices with CNTs deposited on self-assembled monolayer (SAM) passivated oxides,<sup>[8,18]</sup> devices with CNTs overgrown by a top gate oxide,<sup>[16]</sup> and devices passivated with fluoropolymers.<sup>[10,15,17]</sup> A comparison table is given in the Supporting Information. Interestingly, devices with electrodes on top of CNTs placed on SAM passivated SiO<sub>2</sub> require an additional hydrophobic packaging to remove hysteresis,<sup>[17]</sup> whereas devices with electrodes on top of CNTs based on SAM passivated Al<sub>2</sub>O<sub>3</sub> show long-term hysteresis-free behavior without additional packaging.<sup>[18]</sup> In contrast, for devices with CNTs on top of electrodes, a hydrophobic packaging seems to be mandatory to eliminate hysteresis as observed in this work as well. We have also evaluated the transconductance curves measured after a week under ambient condition storage (final) with respect to on-state conductance, on/off ratio, mobility, and subthreshold slope. Figure 4a shows on-state conductance values up to 10<sup>-6</sup> S and on/off ratio up to 10<sup>7</sup>, with no correlation to the h-BN and Teflon layer thicknesses. Considering the small number of 1–5 SWCNTs per device and the 30 fA current detection limit, we conclude that the performance is comparable with previous devices on DEP-deposited polymer-wrapped SWCNTs.<sup>[40]</sup> Also, field-effect mobilities<sup>[56]</sup> up to 100 cm<sup>2</sup> V<sup>-1</sup> s<sup>-1</sup> and subthreshold slopes<sup>[56]</sup> down to 140 mV dec<sup>-1</sup>, as shown in Figure 4b,c, are evidence for the good performance of liquid-phase sorted, polymer-wrapped SWCNTs embedded in h-BN and Teflon.

In summary, we have observed nearly hysteresis-free transconductance curves for (9,8) SWCNTs embedded in h-BN/PTFE heterolayers. The reduction of hysteresis after PTFE coating over a timescale of days has been explained by slow repelling of residual water molecules that strongly adhere to the metallic electrodes onto which nanotubes have been deposited under ambient conditions. Longer waiting times are expected to eliminate hysteresis completely. However, Teflon coating without breaking the annealing vacuum appears to be a more promising route to be explored.

See Supporting Information for reference devices fabricated on Si/SiO<sub>2</sub>, optical and scanning electron micrographs of synthesized h-BN, and a comparison of the measured hysteresis with the literature.

## Supporting Information

Supporting Information is available from the Wiley Online Library or from the author.

## Acknowledgements

S.K. acknowledges funding by the Deutsche Forschungsgemeinschaft (DFG). F.H. and R.K. acknowledge support by the Helmholtz Society through the program, Science and Technology of Nanosystems (STN), and by the Karlsruhe Nano Micro Facility (KNMF).

## Conflict of Interest

The authors declare no conflict of interest.

## Author Contributions

The experiments were conceived and designed by S.K. and R.K. The nanotube raw material was provided by L.W. and Y.C., and purified and length fractionated by F.H. h-BN layers were synthesized by S.K. and the devices were fabricated by S.K. and S.D. C.D. performed the XPS measurements, all other measurements by S.K. and D.D. The manuscript was written by R.K. and S.K. with input from all coauthors.

## Keywords

boron nitride, carbon nanotubes, hysteresis, polytetrafluoroethylene, transistors

Received: April 20, 2020

Revised: May 26, 2020

Published online:

- [1] S. J. Tans, A. R. M. Verschueren, C. Dekker, *Nature* **1998**, 393, 49.
- [2] R. Martel, T. Schmidt, H. R. Shea, T. Hertel, P. Avouris, *Appl. Phys. Lett.* **1998**, 73, 2447.
- [3] M. Rinkio, A. Johansson, G. S. Paraoanu, P. Törmä, *Nano Lett.* **2009**, 9, 643.
- [4] W. Kim, A. Javey, O. Vermesh, Q. Wang, Y. Li, H. Dai, *Nano Lett.* **2003**, 3, 193.
- [5] Y. Pascal-Levy, E. Shifman, M. Pal-Chowdhury, I. Kalifa, T. Rabkin, O. Shtempluck, A. Razin, V. Kochetkov, Y. E. Yaish, *Phys. Rev. B* **2012**, 86, 115444.
- [6] A. Vijayaraghavan, C. W. Marquardt, S. Dehm, F. Hennrich, R. Krupke, *Carbon* **2010**, 48, 494.
- [7] S. H. Jin, A. E. Islam, T. Kim, J. Kim, M. A. Alam, J. A. Rogers, *Adv. Funct. Mater.* **2012**, 22, 2276.
- [8] R. T. Weitz, U. Zschieschang, F. Effenberger, H. Klauk, M. Burghard, K. Kern, *Nano Lett.* **2007**, 7, 22.
- [9] M. Ganzhorn, A. Vijayaraghavan, A. A. Green, S. Dehm, A. Voigt, M. Rapp, M. C. Hersam, R. Krupke, *Adv. Mater.* **2011**, 23, 1734.
- [10] J. Lefebvre, J. Ding, Z. Li, F. Cheng, N. Du, P. R. L. Malenfant, *Appl. Phys. Lett.* **2015**, 107, 243301.
- [11] L. Chua, J. Zaumseil, J. Chang, E. C.-W. Ou, P. K.-H. Ho, H. Sirringhaus, R. H. Friend, *Nature* **2005**, 434, 194.
- [12] S. P. Schießl, N. Fröhlich, M. Held, F. Gannott, M. Schweiger, M. Forster, U. Scherf, J. Zaumseil, *ACS Appl. Mater. Interfaces* **2015**, 7, 682.
- [13] C. Cao, J. B. Andrews, A. D. Franklin, *Adv. Electron. Mater.* **2017**, 3, 1700057.
- [14] H. Shimauchi, Y. Ohno, S. Kishimoto, T. Mizutani, *Jpn. J. Appl. Phys.* **2006**, 45, 5501.
- [15] S. Jang, B. Kim, M. L. Geier, P. L. Prabhuramirashi, M. C. Hersam, A. Dodabalapur, *Appl. Phys. Lett.* **2014**, 105, 122107.

- [16] R. S. Park, G. Hills, J. Sohn, S. Mitra, M. M. Shulaker, H.-S. P. Wong, *ACS Nano* **2017**, *11*, 4785.
- [17] T. J. Ha, D. Kiriya, K. Chen, A. Javey, *ACS Appl. Mater. Interfaces* **2014**, *6*, 8441.
- [18] R. T. Weitz, U. Zsehiesehang, A. Forment-Aliaga, D. Kälblein, M. Burghard, K. Kern, H. Klauk, *Nano Lett.* **2009**, *9*, 1335.
- [19] R. A. Erb, *J. Phys. Chem.* **1965**, *69*, 1306.
- [20] W. R. Tyson, W. A. Miller, *Surf. Sci.* **1977**, *62*, 267.
- [21] Z. Xu, Y. Gao, C. Wang, H. Fang, *J. Phys. Chem. C* **2015**, *119*, 20409.
- [22] X. Ma, S. Cambré, W. Wenseleers, S. K. Doorn, H. Htoon, *Phys. Rev. Lett.* **2017**, *118*, 027402.
- [23] M. Gaulke, A. Janissek, N. A. Peyyety, I. Alamgir, A. Riaz, S. Dehm, H. Li, U. Lemmer, B. S. Flavel, M. M. Kappes, F. Hennrich, L. Wei, Y. Chen, F. Pyatkov, R. Krupke, *ACS Nano* **2020**, *14*, 2709.
- [24] C. R. Dean, A. F. Young, I. Meric, C. Lee, L. Wang, S. Sorgenfrei, K. Watanabe, T. Taniguchi, P. Kim, K. L. Shepard, J. Hone, *Nat. Nanotechnol.* **2010**, *5*, 722.
- [25] J. W. Huang, C. Pan, S. Tran, B. Cheng, K. Watanabe, T. Taniguchi, C. N. Lau, M. Bockrath, *Nano Lett.* **2015**, *15*, 6836.
- [26] A. Baumgartner, G. Abulizi, K. Watanabe, T. Taniguchi, J. Gramich, C. Schönenberger, *Appl. Phys. Lett.* **2014**, *105*, 023111.
- [27] L. Song, L. Ci, H. Lu, P. B. Sorokin, C. Jin, J. Ni, A. G. Kvasninin, D. G. Kvasninin, J. Lou, B. I. Yakobson, P. M. Ajayan, *Nano Lett.* **2010**, *10*, 3209.
- [28] K. K. Kim, A. Hsu, X. Jia, S. M. Kim, Y. Shi, M. Hofmann, D. Nezich, J. F. Rodriguez-Nieva, M. Dresselhaus, T. Palacios, J. Kong, *Nano Lett.* **2012**, *12*, 161.
- [29] A. Ismach, H. Chou, D. A. Ferrer, Y. Wu, S. McDonnell, H. C. Floresca, A. Covacevich, C. Pope, R. Piner, M. J. Kim, R. M. Wallace, L. Colombo, R. S. Ruoff, *ACS Nano* **2012**, *6*, 6378.
- [30] S. K. Jang, J. Youn, Y. J. Song, S. Lee, *Sci. Rep.* **2016**, *6*, 30449.
- [31] S. M. Kim, A. Hsu, M. H. Park, S. H. Chae, S. J. Yun, J. S. Lee, D.-H. Cho, W. Fang, C. Lee, T. Palacios, M. Dresselhaus, K. K. Kim, Y. H. Lee, J. Kong, *Nat. Commun.* **2015**, *6*, 8662.
- [32] R. Y. Tay, S. H. Tsang, M. Loeblein, W. L. Chow, G. C. Loh, J. W. Toh, S. L. Ang, E. H. T. Teo, *Appl. Phys. Lett.* **2015**, *106*, 1.
- [33] S. Behura, P. Nguyen, S. Che, R. Debbarma, V. Berry, *J. Am. Chem. Soc.* **2015**, *137*, 13060.
- [34] Y. Gong, G. Shi, Z. Zhang, W. Zhou, J. Jung, W. Gao, L. Ma, Y. Yang, S. Yang, G. You, R. Vajtai, Q. Xu, A. H. Macdonald, B. I. Yakobson, J. Lou, Z. Liu, P. M. Ajayan, *Nat. Commun.* **2014**, *5*, 3193.
- [35] Y. Shi, C. Hamsen, X. Jia, K. K. Kim, A. Reina, M. Hofmann, A. L. Hsu, K. Zhang, H. Li, Z. Juang, M. S. Dresselhaus, L. Li, J. Kong, *Nano Lett.* **2010**, *10*, 4134.
- [36] P. J. Fazen, E. E. Remsen, J. S. Beck, P. J. Carroll, A. R. McGhie, L. G. Sneddon, *Chem. Mater.* **1995**, *7*, 1942.
- [37] P. J. Fazen, A. T. Lynch, L. G. Sneddon, J. S. Beck, E. E. Remsen, *Chem. Mater.* **1990**, *2*, 96.
- [38] H. Wang, B. Wang, X.-Y. Quek, L. Wei, J. Zhao, L.-J. Li, M. B. Chan-Park, Y. Yang, Y. Chen, *J. Am. Chem. Soc.* **2010**, *132*, 16747.
- [39] H. Wang, L. Wei, F. Ren, Q. Wang, L. D. Pfefferle, G. L. Haller, Y. Chen, *ACS Nano* **2013**, *7*, 614.
- [40] F. Hennrich, W. Li, R. Fischer, S. Lebedkin, R. Krupke, M. M. Kappes, *ACS Nano* **2016**, *10*, 1888.
- [41] V. Karre, P. D. Keathley, J. Guo, J. T. Hastings, *IEEE Trans. Nanotechnol.* **2009**, *8*, 139.
- [42] L. Qin, J. Yu, M. Li, F. Liu, X. Bai, *Nanotechnology* **2011**, *22*, 215602.
- [43] J. C. Koepke, J. D. Wood, Y. Chen, S. W. Schmucker, X. Liu, N. N. Chang, L. Nienhaus, J. W. Do, E. A. Carrion, J. Hewaparakrama, A. Rangarajan, I. Datye, R. Mehta, R. T. Haasch, M. Gruebele, G. S. Girolami, E. Pop, J. W. Lyding, *Chem. Mater.* **2016**, *28*, 4169.
- [44] M. Corso, W. Auwärter, M. Muntwiler, A. Tamai, T. Greber, J. Osterwalder, *Science* **2004**, *303*, 217.
- [45] P. Sutter, J. Lahiri, P. Albrecht, E. Sutter, *ACS Nano* **2011**, *5*, 7303.
- [46] A. Nagashima, N. Tejima, Y. Gamou, T. Kawai, C. Oshima, *Phys. Rev. B* **1995**, *51*, 4606.
- [47] Y. Gao, W. Ren, T. Ma, Z. Liu, Y. Zhang, W. Bin Liu, L. P. Ma, X. Ma, H. M. Cheng, *ACS Nano* **2013**, *7*, 5199.
- [48] S. Behura, P. Nguyen, R. Debbarma, S. Che, M. R. Seacrist, V. Berry, *ACS Nano* **2017**, *11*, 4985.
- [49] A. L. Gibb, N. Alem, J. H. Chen, K. J. Erickson, J. Ciston, A. Gautam, M. Linck, A. Zettl, *J. Am. Chem. Soc.* **2013**, *135*, 6758.
- [50] J. Lu, P. S. E. Yeo, Y. Zheng, H. Xu, C. K. Gan, M. B. Sullivan, A. H. Castro Neto, K. P. Loh, *J. Am. Chem. Soc.* **2013**, *135*, 2368.
- [51] G. Kim, A. R. Jang, H. Y. Jeong, Z. Lee, D. J. Kang, H. S. Shin, *Nano Lett.* **2013**, *13*, 1834.
- [52] M. K. Yang, *J. Micro/Nanolithogr. MEMS MOEMS* **2008**, *7*, 033010.
- [53] S. Lee, T. Jeong, S. Jung, K. Yee, *Phys. Status Solidi B* **2019**, *256*, 1800417.
- [54] R. Gholami, M. Alyani, K. Smith, *Catalysts* **2015**, *5*, 561.
- [55] M. Shlafman, T. Tabachnik, O. Shtempluk, A. Razin, V. Kochetkov, Y. E. Yaish, *Appl. Phys. Lett.* **2016**, *108*, 163104.
- [56] T. Dürkop, S. A. Getty, E. Cobas, M. S. Fuhrer, *Nano Lett.* **2004**, *4*, 35.